MICROSTRUCTURAL AND THERMAL RESPONSE EVOLUTION OF METALLIC FORM-STABLE PHASE CHANGE MATERIALS PRODUCED FROM BALL-MILLED POWDERS

Chiara Confalonieri[1]*, Paola Bassani[2], Elisabetta Gariboldi[1]

[1] Politecnico di Milano, Dipartimento di Meccanica, Via La Masa 1, 20156 Milano, Italy
[2] National Research Council of Italy, Institute of Condensed Matter Chemistry and Technologies for Energy CNR-ICMATE, Via Previati 1/E, 23900 Lecco, Italy
* E-mail: chiara.confalonieri@polimi.it, telephone number +39 0223998661

Abstract
Phase Change Materials (PCMs) can store and release the latent heat associated to a phase transition, so they can be applied in thermal energy management and storage systems. Among them, form-stable (FS) PCMs can consist of two immiscible phases: an active phase, which undergoes the solid-liquid transition, and a matrix, which provides the structural properties and prevents leakage of the active phase when it is liquid. This experimental study focused on the characterization of a metallic FS-PCMs based on an Al-Sn alloy, obtained by powder metallurgy from ball-milled powders, compacted at room temperature and sintered at 200, 250 and 500°C. The main properties that characterize PCMs are the temperature range over which transition occurs and the associated enthalpy, i.e. the stored energy. Differential Scanning Calorimetry (DSC) is one of the more suitable characterization techniques to evaluate these properties and so the thermal response of PCMs. To check thermal response and its stability, DSC tests including several thermal cycles were conducted. DSC analyses were performed also before and after several thermal cycles simulating possible operative conditions. Moreover, microstructural analysis, through Scanning Electron Microscopy and X-Ray Diffraction, allowed to relate the thermal response variations to microstructural and mechanical changes.

Keywords: metallic Phase Change Materials, form-stable, thermal stability, Differential Scanning Calorimetry, ball milling

Article Highlights
- Al-40%mass Sn alloy was produced by ball-milled powders as form-stable Phase Change Material for thermal energy storage.
- The material shows a solidification temperature broader than melting one, with close enthalpy values.
- The material shows good thermal and mechanical stability during thermal cycles simulating service.

Acknowledgments
The authors would like to thank Aldo Tommaso Grimaldi, for samples production and initial characterization, and Enrico Bassani, for his help in XRD tests.

This work was supported by the Italian Ministry for Education, University and Research through the project Department of Excellence LIS4.0 (Integrated Laboratory for Lightweight e Smart Structures).

1. Introduction
Phase Change Materials (PCMs) for energetic applications are materials which can store the heat associated to a phase transition and release it when the transition is reversed [1]. Thermal energy storage and

management are becoming more and more critical issues in many domestic and industrial applications, especially to minimize and mitigate the environmental impact of energy consumption [1,2]. In this perspective, PCMs can play a significant role and indeed they have been studied and applied in many different sectors: buildings, solar thermal storage systems, solar energy (e.g. solar panels, concentrating solar thermal technologies), heat pumps, electronic devices, smart textiles, biomaterials and biomedical applications, automotive applications, space applications, food industry [1,3–5].
In the selection of PCMs for heat storage applications, the most important thermo-physical properties are the transition temperature and the heat of fusion [1,4,6]. So far, research focused mostly on low-temperature PCMs, i.e. with melting temperature lower than 120-150°C; however, many medium and high-temperature applications, ranging from 120°C to more than 1600°C, can exploit the advantages of using PCMs (e.g. space heating, steam turbine electricity generation, high temperature industrial processes) [2,5,6]. Medium- and high-temperature PCMs can be mainly inorganic compounds (e.g., inorganic salt), metals and alloys, and other uncommon compounds with a medium or high melting temperature [6]. Among them, metallic materials are still the less used class, even if they have many interesting features, like high thermal conductivity, large latent heat per unit volume, good thermal stability and reliability; on the other hand, they have a relatively low latent heat [5–8].
When they exploit a solid-liquid transition, metallic FS-PCMs must keep structural properties as well as prevent active phase leakage. This is mostly achieved by embedding the active phase which undergoes the phase transition (i.e. the actual PCM) in a higher-melting phase which is solid in the whole service temperature range; in some cases, also the high wettability of the active phase on the high-melting phase in the service temperature range is a key factor to ensure the stable form [9].

The most frequently used approach to obtain metallic PCMs is encapsulation (through mechanical process or electroplating); however, these materials tend to oxidize and to degrade at high temperatures, which reduce their durability and thermal energy performance [6]. An alternative approach that has been considered more promising is the use of alloy-based PCMs [6]. In this perspective, Sugo et al. [5,10,11] suggested to exploit Miscibility Gap Alloys (MGAs), to obtain a two-phase mixture in which the two phases are completely immiscible at solid state. Examples of such systems are: Fe-Cu, Fe-Mg, Al-Bi, Al-Sn [5]; the phase diagram of Al-Sn is shown in Fig 1. This approach allows to keep a stable composition over time and thermal cycles, by preventing the formation of intermetallics or solid solutions. This is possible if the high-melting alloy has low solubility in the active phase also when the latter is in the molten state. However, simple cooling of a molten MGAs results in active phase solidification around the matrix grains, which is opposite to the desired microstructure. One of the possible solutions is the use of powder metallurgy processes (powder mixing, compression and sintering), that can provide a proper microstructure with fine distribution of active phase particles inside the matrix [5,12]. Gariboldi and Perrin followed this approach to obtain Al-Sn based PCMs starting from simple mixed powders, as suggested by Sugo et al. [5,13]. The difference between the two works is that Gariboldi and Perrin performed not only room temperature compression, but also hot compression, which in principle allows to avoid a further sintering process. The current work is an attempt to further improve the properties of Al-Sn based PCMs by applying ball milling as mixing technique.

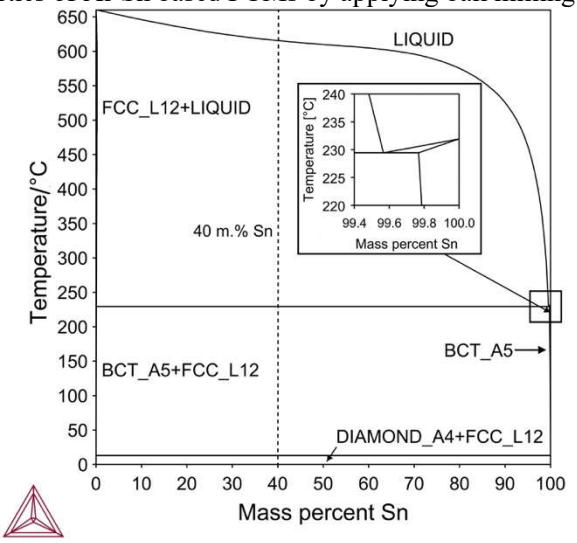

Fig 1 Al-Sn phase diagram with considered composition (computed using Thermo-Calc Software TCAL6 Aluminium-based alloys database, accessed 24th July 2019). The inset shows the eutectic reaction occurring at 228°C around 99.6 mass% Sn.

Ball milling (BM) is the most common comminution technique to obtain fine particles from solids. In its simplest form, it consists of a rotating hollow cylinder, partially filled with balls (grinding media), with its axis either horizontal or at a small angle to the horizontal: the impact of the balls against each other grinds the material trapped between them. This simple, but effective technique can be applied to metals, ceramics, polymers and composite materials [14]. When mixtures of metallic powders are milled together, the process is called Mechanical Alloying (MA) [14]. Two simultaneous events occur: power size is reduced and a homogeneous alloy is obtained, thanks to the material transfer during the process [14]. In facts, powders are milled until they reach a stable state in which every powder particle has composition corresponding to the proportion of the elements in the starting powder mix [14]. This allows to obtain non-equilibrium microstructures, like homogeneous and finely dispersed MGAs [12,14]. This process was successfully applied by Liu et al. [12] to produce Al-Sn alloys for bearings, which have an ideal microstructure similar to the desired one. Therefore, the expected advantages are a finer microstructure, which could reduce molten Sn leakage during transition, and higher hardness with respect to conventional powder metallurgy processes with simple mixing of powders. Promising results in this direction were obtained by the authors in a first comparison of ball-milled cold-compressed samples to simple-mixed ones [15]. On the other hand, simple mixing is a simpler and cheaper process.

Considering PCM characterization, composition, structure and phase amounts should be evaluated through microscopy (optical and scanning electron microscopy) and X-ray diffraction (XRD), since thermal effect and efficiency are related to them. Then, Differential Scanning Calorimetry (DSC) can be used to analyse thermal response of the material. In DSC, a phase transition can be detected through a peak in heat flow signal, therefore this technique is usually applied to determine at the same time its temperature range (peak position and width) and its latent heat (peak area) [7]. Moreover, also the peak shape is important, since it reflects the rate (time dependent or temperature dependent) at which thermal energy is stored or released. A possible drawback of DSC technique is that sample size should be selected sufficiently large to be representative of the entire system (matrix + PCM) and, at the same time as small as possible to avoid peak broadening, especially in materials with relatively poor thermal conductivity [8,16]. MGAs usually have a homogeneously distributed microstructure at the millimetre scale size, therefore a small specimen can be considered as representative of the whole material. In this way, it is possible to consider interface effects that could not be evaluated when only the active phase is tested. Nevertheless, thermal characterization by DSC analyses should be combined with functional tests which simulate service conditions, i.e. series of thermal cycles around transition temperature, to check thermal stability as well as presence and effects of leakage. In the case of FS-PCMs, the mechanical behaviour and its stability after thermal cycles that simulate service should be assessed to exploit PCM-containing materials in structural applications.

In this study, an Al-40% mass Sn alloy, which corresponds to 20% Sn in volume, is proposed as PCM. The transition temperature of this alloy is close to Sn melting temperature, i.e. ~230°C, therefore it can be considered as a medium-temperature PCM. Samples were produced by powder metallurgy after ball milling of powders. Then, microstructural, thermal, mechanical and functional characterization was conducted, with focus on thermal and mechanical stability over several thermal cycles.

2. Materials and experimental procedures

2.1 Material production

Al and Sn powders were selected to produce sample by powder metallurgy. The Al powder was an atomized high purity Al (> 99.7 mass%) powder with diameters smaller than 45 µm (ECKA Granules GmbH, Germany). The Sn powder (SN, Metalpolveri S.r.l) was characterized by high purity (Sn > 99.9 mass%), very fine particle-size distribution (Over Sieve Grain Size: <25µm 64÷71%, 25µm<OSGS<45µm 20÷26%, 45µm<OSGS<75µm 5÷11%, >75µm <0.3%) and good homogeneity.

Sn powder was mixed to Al powder to get nominal volumetric composition of the alloy equal to 80% Al and 20% Sn (corresponding to about 40 mass% Sn, as shown in Fig 1). Then, the blend was ball-milled using a planetary mill (Retsch PM 400 Planetary Ball Mill), sealing the mixed powder in stainless steel jar together with hardened steel balls of diameter 20 mm (material to ball mass ratio 1:5, about 80% of empty space in the jar). Ethanol was added as lubricant (40% on the total weight of powders) to avoid cold fusion phenomena [12]. Moreover, the process was performed in pure Ar atmosphere to achieve protection from oxidation. Powders were ground for 24 hours at 250 rpm, alternating grinding cycles of 20 minutes to pause cycles of 10 minutes to avoid excessive increases in temperature due to friction and to further minimize oxidation phenomena.

Finally, cylindrical samples were obtained by cold compression (CC) and sintering of powders, using the same parameters and procedures applied in the previous study by Gariboldi and Perrin [13], in which powders

were simply mixed before the densification stage. About 23 g of ball-mixed powders were compressed at room temperature using an Instron 1195 100kN Universal Testing Machine equipped with an extrusion set consisting of a hollow cylinder steel die and a 15 mm diameter punch. In order to obtain a good densification, compression was divided into three steps: pre-compression up to 20 kPa, compression up to maximum pressure, i.e. 300 MPa, and, after a pause of 60 s to allow relaxation of the structure, final compression up to maximum pressure. A set of samples with diameter of 15 mm and height of about 15 mm were thus obtained. After densification, samples were longitudinally cut in smaller parts and sintered in Carbolite TZF 12/75/700 Furnace in pure Ar atmosphere at 220°C (CC220), 250°C (CC250) or 500°C (CC500) for 1 hour or at 500°C for 5 hours (CC500-5h). Sintering temperatures of 220°C and 250°C are commonly used in the production of bearing alloys [17], while sintering at 500°C was proposed by Sugo et al. for metallic Al-Sn PCMs [5]. Then, samples slowly cooled down to room temperature in the furnace, keeping the Ar atmosphere. Sintering is necessary for CC samples to assure cohesion of the solid and therefore the desired mechanical and physical properties [18]. The sample CC500 was tested to simulate service conditions by cycling it 100 times in air between 175°C and 285°C, thus including the melting/solidification temperature range of the active phase. Sample was inserted and removed from Carbolite TZF 12/75/700 Furnace, using a thermocouple to monitor its temperature.

Microstructural, thermal and mechanical features were evaluated with the following characterization techniques.

2.2 X-ray diffraction

Crystalline phases were verified by X-ray diffraction (XRD) analyses, performed with Panalytical X'Pert PRO MPD X-ray diffractometer (θ-θ geometry, Cu Kα source) at room temperature on pure element powders (Al, Sn), ball-mill mixed powders, as-compressed powders, as-sintered samples and on the sample subjected to thermal cycles. The identification of crystalline phases was performed comparing the patterns with references from the Crystallography Open Database [19,20] using Maud software [21].

2.3 Microstructural characterization

After each step of processing above the melting temperature of Sn and after simulated service, the absence/presence of Sn leakage was observed visually or at low magnification.

The microstructural characterization after conventional metallographic preparation was carried out by Scanning Electron Microscopy (SEM, Zeiss EVO 50) and high-resolution Field Emission Gun Scanning Electron Microscopy (FEG-SEM, Hitachi SU70) on as-sintered samples and on selected sample after thermal cycles. A semiquantitative analysis of the composition was conducted using the Energy Dispersive X-ray Spectrometry (EDS) detector of the same FEG-SEM. Since Al and Sn have a significant Z-contrast, the presence and shape of Al and Sn phases are clearly highlighted without any etching in SEM micrographs obtained by Backscattered Electrons (BSE).

2.4 Mechanical characterization

Mechanical characterization on samples in different conditions was done by Vickers microhardness tests on Future-tech FM-700 microhardness tester. Five indentations were done for each specimen, with 4.91 N load on the indenter and dwell time of 15 s.

2.5 Thermal characterization

Differential Scanning Calorimetry (DSC, DSC Seiko 220 C) analyses were performed to evaluate the stability of PCM thermal behaviour and amount of energy stored over thermal cycles. DSC tests were conducted in Al pans on pure element powders (Al 22.73 mg, Sn 33.79 mg) and on sample CC500 before and after 100 thermal cycles (samples of 46.3 mg were obtained in both cases from central regions of the cylinder). DSC test cycle consisted in heating and cooling the sample with the same rate from room temperature to 320°C, repeating the cycle several times. Three different heating/cooling rates were applied (5°C/min, 10°C/min, 20°C/min). Each testing condition was repeated with empty pans to obtain the zero line [22]; these curves were subtracted to samples' heat flow curves during the data analysis step, in order to remove possible effects due to the instrument. Some consecutive DSC cycles were carried out both on as-sintered sample CC500 and after 100 cycles of its simulated service in external furnace (Thermally Cycled, CC500-TC). During each set of consecutive cycles, both samples were not removed from DSC pan.

The stored/released energy was conventionally evaluated measuring the area of the transition peak associated to the melting/solidification of Sn in the Heat Flux vs. Time curve; the baseline in correspondence of the peak was interpolated as linear [22]. Considering the melting peak, onset and offset temperature were determined as the temperature values corresponding to threshold values of the derivative (0.005 or -0.005, respectively), i.e. when the curve is not anymore horizontal, or it becomes horizontal again after the peak. The melting peak temperature was evaluated as the minimum of the heat flow curve. Considering the solidification peak, only a visual analysis was conducted, due to its very complex shape.

3. Results

3.1 X-Ray Diffraction

XRD patterns of powders (Fig 2) show that the two pure element powders contain only Al and the body-centred tetragonal β-Sn [20]. These phases were the only ones detected also after ball milling and further sintering processes at different temperatures (Fig 3). In addition to them, after thermal cycles simulating service, the presence of Sn oxide can be observed in Fig 3. As shown in the inset of both figures (Fig 2, Fig 3), peak broadening occurred during ball milling.

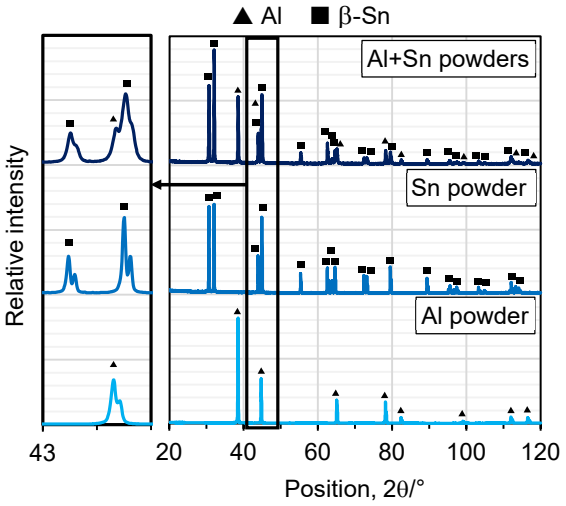

Fig 2 XRD pattern of pure Al powder, pure β-Sn powder and ball-mill mixed Al and Sn powders. In the inset, a magnification of peaks at 2θ = 43÷45° is shown.

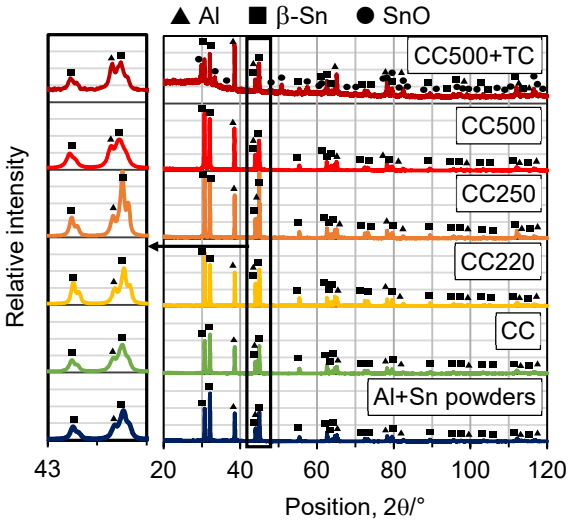

Fig 3 XRD pattern of ball-mill mixed Al and Sn powders, cold-compressed sample (CC), sintered samples (CC220, CC250, CC500) and thermally cycled sample (CC500+TC). In the inset, a magnification of peaks at 2θ = 43÷45° is shown.

3.2 Microstructure

Visual analysis highlighted Sn leakage during sintering, while no leakage occurred during the following thermal cycles. The effect of process parameters and simulated service on microstructure is clearly shown by SEM micrographs (Fig 4, Fig 5), where the white phase is the Sn-rich phase and the darker one is the Al-rich phase. In samples CC220, CC250 and CC500 (Fig 4-a,b,c), it is possible to observe fine Sn particles, with random orientation, and coarse Sn particles, generally oriented perpendicularly to compression direction (vertical). At low-magnification level, the microstructure is similar at sintering temperatures of 220 and 250°C, while at 500°C the size of coarse Sn particles reduces. High magnification micrographs clearly show the change of Sn distribution as sintering temperature increases, with the progressive reduction of coarse Sn particles in favour of finely dispersed Sn particles. A longer sintering time (Fig 4-d) causes more evident modifications in the microstructure: particle orientation is almost lost and the presence of regions with finely dispersed Sn particles increases. Moreover, there are coarse (50÷70 μm) Sn particles with some Al fine particles (100÷200 nm) inside. Pores were not observed in any sample.

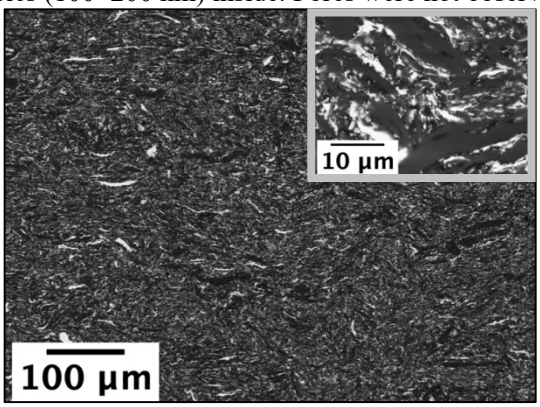

a)

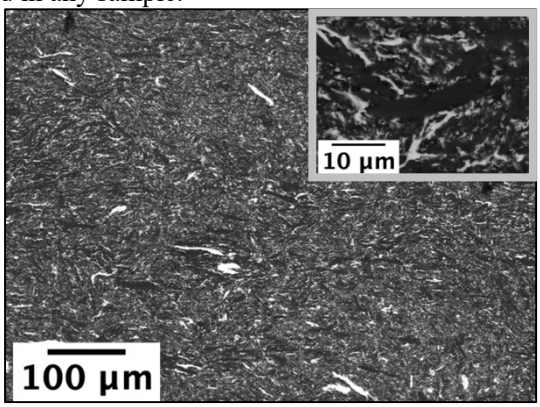

b)

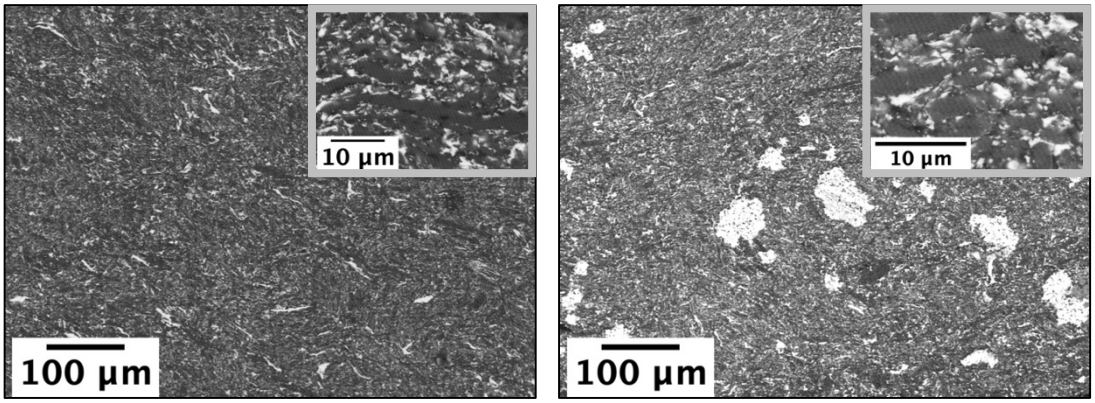

c) d)

Fig 4 SEM-BSE micrographs of samples CC220 (a), CC250, CC500 (c) and CC500-5h (d). Compression direction during compaction process: vertical. Higher magnification micrographs are shown in boxes at top right corner of each image.

Sample CC500 was selected for thermal stability analyses. This sample is more homogeneous than the ones sintered at lower temperatures and it does not have coarse Sn particles as sample CC500-5h; moreover, shorter sintering temperature is better in industrial perspective.

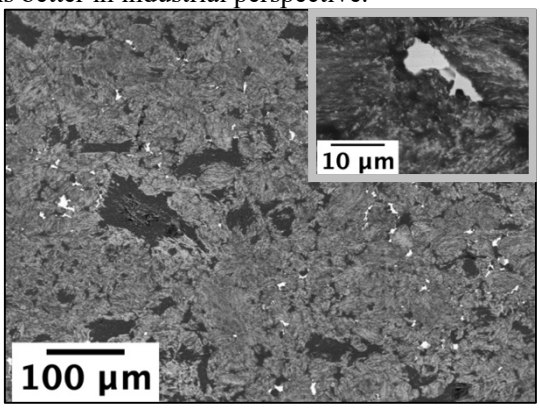

Fig 5 SEM-BSE micrographs of sample CC500 after 100 thermal cycles (CC500-TC). Compression direction during compaction process: vertical. Higher magnification micrograph is shown in boxes at top right corner of image.

After 100 thermal cycles simulating service conditions, a microstructural modification occurred on sample CC500 sample (CC500-TC). At relatively low magnification (Fig 5), it is still possible to observe relatively coarse Sn particles (smaller than 20 µm) and Al grains with sub-micrometric Sn particles inside, but most of the microstructure has an intermediate composition. To investigate such microstructure, high-resolution FEG-SEM images of sample CC500 before and after thermal cycles are compared in Fig 6. It can be observed that the region which is light grey in Fig 5 is characterized by an extremely fine distribution of sub-micrometric Al and Sn particles at Al grain boundaries, which was already present in a smaller extent before thermal cycles (see arrows in Fig 6-a,b). On the other hand, both Al and Sn coarse particles became smaller, resulting in a more homogeneous microstructure. Even on these higher resolution images, measurement of the fine Sn particles size is difficult (Fig 6-c,d); anyway, qualitative observations suggest a broad particle size distribution, with the presence of both micrometric and sub-micrometric particles.

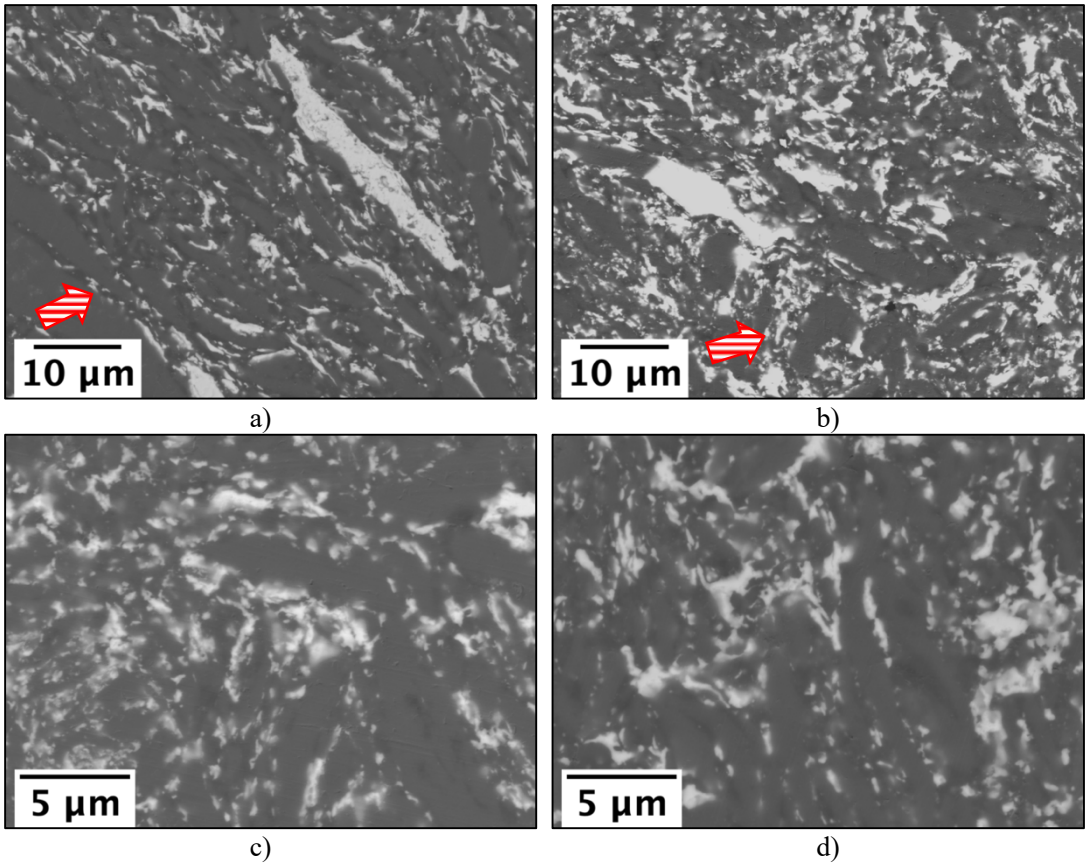

Fig 6 FEG-SEM BSE micrographs of sample CC500 before (a,c) and after (b,d) 100 cycles; arrows in a,b highlight the fine microstructure at the boundary of Al particles.

Concerning composition, EDS analysis revealed variations in the alloy composition. The average of four measurements, each on area of about 0.3 mm^2, gave Sn/Al percentages of 0.62, 0.57 and 0.49 for ball-milled powders, samples CC500 and CC500-TC respectively, which suggest in any case a lower value compared to the nominal ratio of 0.67. Also, a non-negligible amount of O was detected in ball milled powders as well as in sample CC500 before and after thermal cycles. It can be observed from EDS profiles of sample CC500 as produced (Fig 7) that O is more present in Sn regions, especially on the boundaries of the smaller particles.

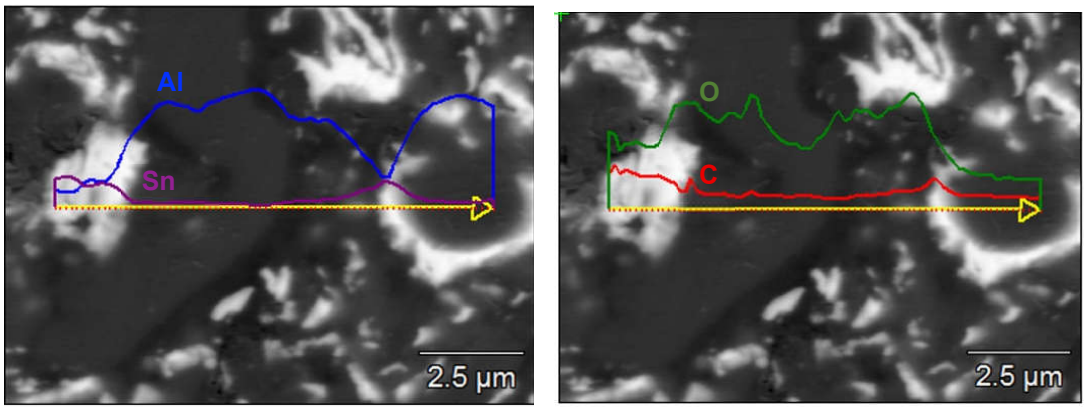

Fig 7 EDS profiles of sample CC500 in the as-sintered condition. Lines in a) refer to Al (blue) and Sn (purple), those in b) to O (green) and C (red).

3.3 Mechanical properties

Results of Vickers micro-hardness tests are summarized in Fig 8. Different sintering temperatures do not significantly affect HV according to any clear trend, confirming the similarity of the three samples already highlighted from microstructures. Both longer sintering time value and thermal cycles seem to increase hardness of sample CC500; however, HV of this sample has a wide standard deviation, which means that this effect is not so significant.

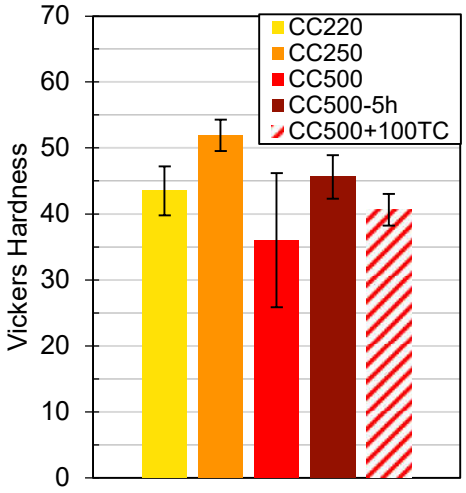

Fig 8 Results of Vickers micro-hardness tests on as-produced samples (CC220, CC250, CC500, CC500-5h) and on sample CC500 after 100 thermal cycles (CC500+TC).

3.4 Thermal properties

DSC curves of homogeneous Al powder do not show relevant features in the temperature interval of interest, i.e. up to about 300°C. On the other hand, the DSC curves at different heating/cooling rates of Sn homogeneous powder display a regular V-shape peak in heating (Fig 9), which changes in height and width depending on the heating rate, as expected. Focusing on the cooling part of the curves, the main solidification peak overlaps secondary smaller peaks. The latent heat for Sn melting and solidification is 52.7±0.1 J/g and 52.3±0.1 J/g, respectively; these values are the average of the ones for the four cycles.

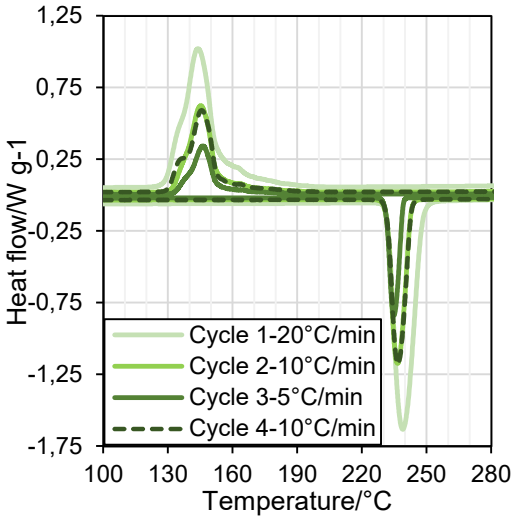

Fig 9 Melting and solidification peaks of pure Sn subjected to consecutive thermal cycles inside DSC machine at different heating/cooling rates (5°C/min, 10°C/min, 20°C/min).

Melting and solidification peaks in DSC curves of sample CC500 tested before and after 100 cycles of simulated service are shown as function of temperature in Fig 10 and Fig 11, respectively; the heating/cooling rate of the selected cycles was 20°C/min, but analogous results were obtained at different heating/cooling rates. As in the case of pure Sn powder, the melting peak (Fig 10) has a regular V-shape, which displays only minor changes in curve slopes and peak values even after 100 cycles. As expected, decreasing heating rate, the peak temperature decreases as well and peak broadens, with higher offset temperatures; after thermal cycles, peak width is smaller. Solidification peak (Fig 11) consists of several superimposed peaks, the main one at about 140-150°C. These peaks progressively change with cycles, specifically during the first ones, performed on the as sintered specimen. After 100 cycles, the shape of heat flow curve in cooling is quite stable.

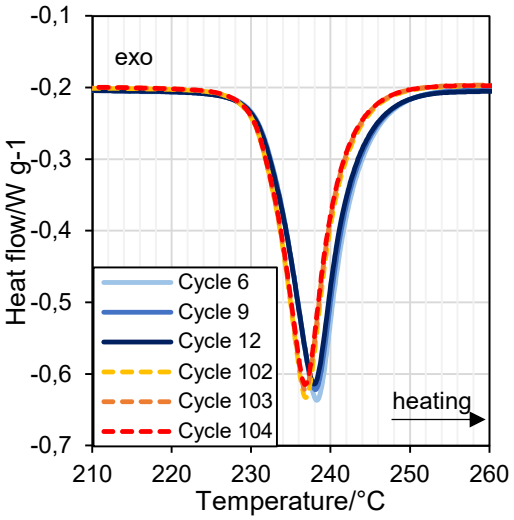

Fig 10 Melting peak of selected consecutive thermal cycles inside DSC machine at 20°C/min heating rate, before (cycle 6÷12) and after external thermal cycles (overall cycle 102÷104).

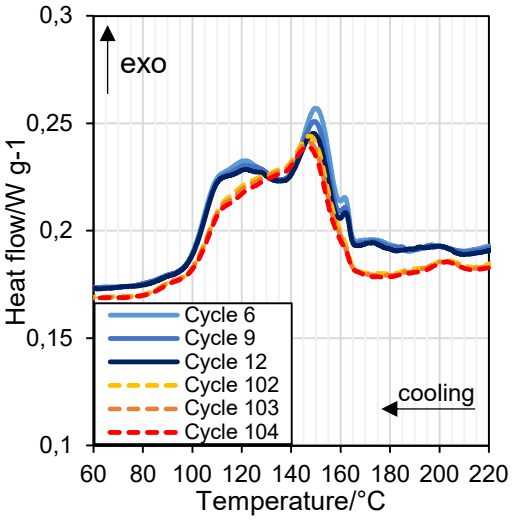

Fig 11 Solidification peak of selected consecutive thermal cycles inside DSC machine at 20°C/min cooling rate, before (cycle 6÷12) and after external thermal cycles (overall cycle 102÷104).

Comparing the solidification peak at different cooling rates (Fig 12), it can be observed that at low cooling rates the narrower peak between 160°C and 165°C in as-sintered samples is particularly evident. The same peak tends to disappear with thermal cycles. Further, it is possible to notice that the wide peak starting at about 200°C disappears as well. On the other hand, the main peak at 150°C becomes larger and sharper; also, the part of the peak between 100°C and 140°C reduces. Also, in this case, the peak broadening increases with heating rate.

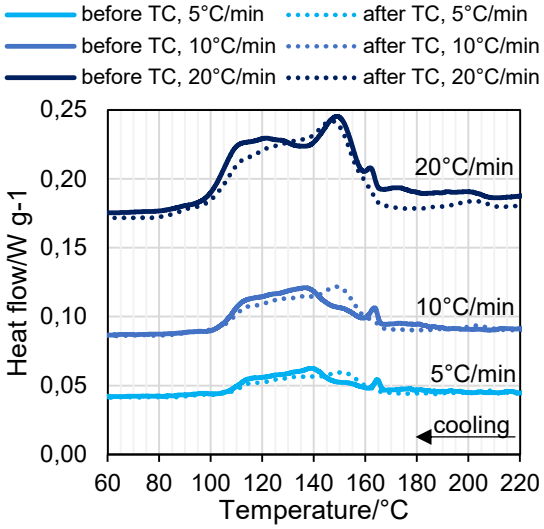

Fig 12 DSC curves at different cooling rates of solidification peaks before and after 100 thermal cycles (TC).

The peak area corresponding to the energy stored and released during the phase transition was measured, resulting in a value around 9 J/g. Considering the complex shape of the solidification peak, it was not so trivial to determine peak onset and offset, which selection should have led in any case to relatively small differences in melting/solidification enthalpy. These, summarized in Fig 13 and Fig 14, show close values at different heating/cooling rate and a slight decrease of enthalpy after 100 thermal cycles.

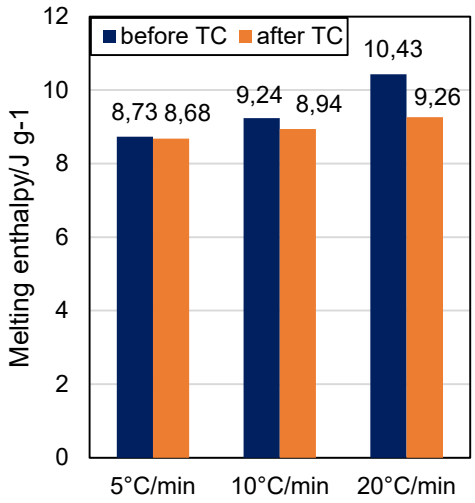

Fig 13 Melting enthalpy of sample CC500 before and after 100 thermal cycles (TC).

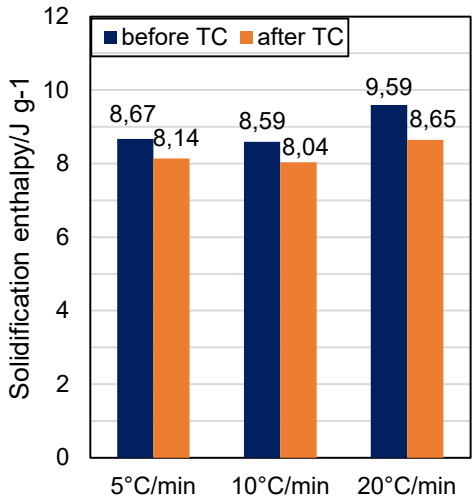

Fig 14 Solidification enthalpy of sample CC500 before and after 100 thermal cycles (TC).

Analysing the changes in enthalpy with thermal cycles and heating rates (Fig 15), a clear decreasing trend for both melting and solidification enthalpy during the first 10 cycles is observed. After 100 cycles, further reductions can be noticed especially in solidification, even if they are less significant. Considering transition temperature, the onset of melting peak is at about 228°C, with minimal increase with heating rate and only smooth reduction after thermal cycles (Fig 16). In facts, repeated DSC cycles at 20°C/min heating/cooling rate show an experimental scatter in melting onset of the order of 0.5°C. In solidification, experimental scatter of onset temperature is higher, and no clear trend can be given for the variation in the first cycles, while thermal cycling clearly reduces the onset temperature.

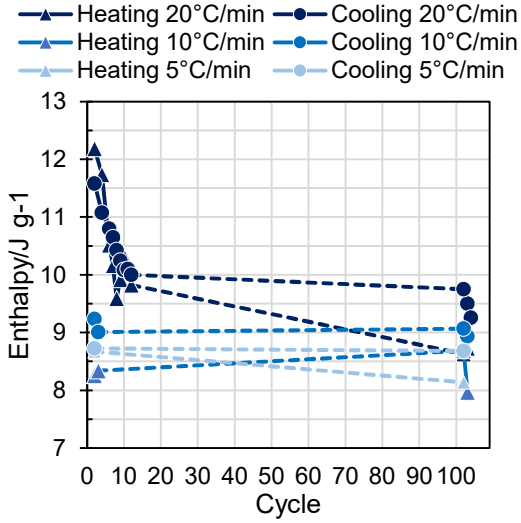

Fig 15 Melting and solidification enthalpy as function of cycle number at different cooling rates.

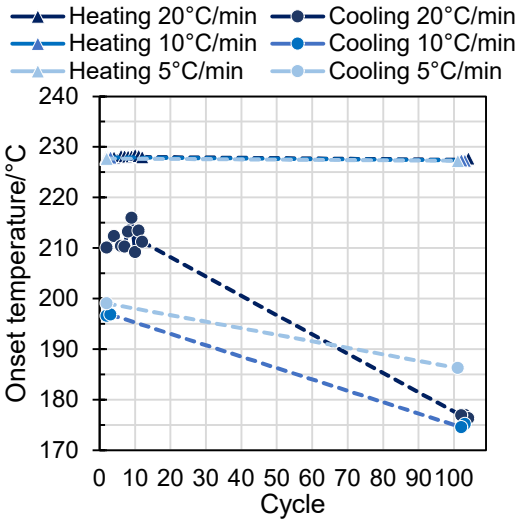

Fig 16 Melting and solidification onset temperature as function of cycle number at different heating rates.

4. Discussion

4.1 Alloy structure and mechanical properties

The analysis of XRD peaks suggests that ball-milling process as well as the following sintering treatments at different temperatures/times have not induced the presence of phases in addition to the expected Al and β-Sn ones. In facts, Sn exists in four allotropic forms: diamond-like α-phase (below 13°C, at room pressure), body-centred tetragonal β-phase with two atoms in the basis (13.2÷232°C, at room pressure), body centred tetragonal γ-phase (room temperature, pressure 9.4÷45 GPa) and body-centred cubic σ-phase (room temperature, pressure > 45 GPa) [23,24]. Since α-phase unit cell has a higher volume than β-phase one [25], its formation is unlikely under the pressures arisen during both ball milling and compression. On the other

hand, such pressures can be estimated to be significantly lower than the ones inducing high-pressure phase transitions.
Further, XRD results display peaks corresponding to SnO only on the sample thermally cycled in air (CC500-TC). However, EDS highlighted the presence of O also on sample CC500. The situation is similar to that observed and explained by Navarrete et al. [26], i.e. many nanoparticle production processes cause the formation of an extremely thin layer of amorphous Sn oxide (~10 nm, regardless of particle size) on nanoparticle surface, which, during following heat treatment, crystallises becoming visible in XRD spectra. In the present case, thermal cycling in air could also have enhanced the formation of SnO. This is confirmed by minor changes of melting enthalpy with thermal cycling, suggesting that only small amount of Sn, by forming the mentioned oxide, was no more available to store/release energy in the PCM material. This drawback could be mitigated when considering industrial parts made of this material, thanks to lower surface to volume ratio as well as the possibility to apply surface treatments or protection methods to avoid oxidation.
In as-produced samples, the PCM alloy microstructure is characterized by the presence of both coarse and fine (submicrometric) Sn particles, these latter prevailing as increasing sintering temperature and time. The increased amount of finely dispersed Sn particles could be correlated to the reduction of Al solubility in the molten phase reached when the material was sintered or cycled below 250°C.
The Sn phase distribution in sample CC500 was qualitatively observed to evolve during simulating service: the biggest particles shrinkage, new small particles form and already present fine Sn particles coarsen. In this microstructure, the non-interconnected Sn particles can be considered encapsulated in Al matrix and, so, molten Sn leakage can occur only from coarse Sn particles at the surface or directly interconnected to it. It is reasonable to expect that a similar microstructure forms in other samples produced from ball-milled powders due to mechanical alloying effect of ball milling that can enhance Al diffusion inside molten Sn.
The presence of many finely dispersed Sn particles has a beneficial effect on hardness, due to the dispersion of the soft sub-micrometric Sn particles in the Al matrix, i.e. dispersion hardening [17]. While in the ball-milled and compressed Al-40%m Sn samples of the present study hardness was about 40 HV (Fig 8), the hardness of simple-mixed samples produced with same starting powders, same nominal composition and compressed with similar parameters by Gariboldi and Perrin [13] was about 30 HV.

4.2 Thermal properties

The sequence of DSC tests on the Sn powder suggest that the shape of melting peak is independent of the number of cycles. On the other hand, while the height of the main cooling peak is only dependant on the cooling rate, the shape of secondary peaks is related to cycle repetitions. This is clear when the peaks obtained at 10°C/min cooling rate are compared (Fig 9), since the 4th cycle displays a clearer secondary peak on the left of the main one. It was not possible to find in literature comparable results of DSC tests on metal powders, therefore a possible explanation of the presence of secondary solidification peaks is given according to thermodynamic considerations. Since molten Sn has a low wettability on the Al pan [9], it is possible to suppose that initially only few particles can nucleate heterogeneously on the pan (very small peak on the right in Fig 9), then homogeneous nucleation can occur allowing solidification of most Sn (biggest peak). The secondary peak at lower temperature could be due to some Sn droplets that remained isolated from the rest of the Sn mass, which hindered their nucleation; this condition can happen randomly in every cycle. Despite the modifications in peak shape, the latent heat of powders is independent of the cycle number, at least for a few cycles. However, the measured (~ 52 J/g) value is lower than the ones reported in literature, i.e. ~ 60 J/g [5,26,27].
Sample CC500 displayed a quite stable onset melting temperature, that can be considered as the activation temperature for PCM. This value, of about 228°C, is slightly lower than the one of pure Sn melting temperature (232°C) according to the phase diagram (Fig 1) and literature [23]. This is probably correlated to the occurrence of Al-Sn eutectic reaction, which takes place at 228°C, as shown in Al-Sn phase diagram (Fig 1). The V-shaped melting peak, spanning over 10-20°C for the investigated heating rates and repeated thermal cycles, indicates the possibility of a relatively fast and repeatable heat storage for the material subjected to these thermal cycles.
On the other hand, DSC curves reveal a completely different solidification behaviour of these samples: significant undercooling ranging from about 20°C to 50°C is observed. Further, the onset temperature and the shape of the broad solidification peak in DSC curve are less stable. As a matter of fact, the shape of this peak, and thus its changes over repeated cycles, are related to the particle size distribution. In a study about solidification of Sn droplets in an aluminium matrix, Kim and Cantor [28] observed a similar DSC curve and analysed Sn particle size using a TEM: they proved that solidification of the larger particles (size > 100 nm) occurred with lower undercooling, at the first peak, while smaller particles (size < 100 nm) solidified at a lower temperature peak. Heterogeneous nucleation sites at the droplet/matrix interface were also proved to

change the solidification temperature [28]. Similarly, it is possible to assume that, in the present case, coarse Sn particles solidify between 200°C and 165°C, while sub-micrometric particles solidify at lower temperatures (160÷100°C), resulting in the observed multiple solidification peak. Also, the evolution of the broad and complex solidification peak could be explained on the above basis: as coarse particle size decreases with thermal cycles, the peaks at higher temperatures tend to disappear. At the same time, lower-temperature part of this complex thermal event (ranging from 140 to 100°C) tends to reduce in height and to move at higher temperatures, towards the peak observed at 150°C for cooling rate 20°C/min. This behaviour, particularly evident in tests carried out at 5 and 10°C/min, can be explained by a progressive coarsening of fine particles. Further changes of solidification peak shape with the number of thermal cycles simulating service cannot be easily predicted. In any case, it seems reasonable that many more than 100 thermal cycles simulating service will be needed to completely remove coarse Sn particles and conclude fine particles coarsening to significantly change the shape of solidification DSC curve. This means that only small reduction of the broad solidification peak is expected, with the result that most of the energy release for this material will mostly occur within the 160-110°C range, like in the experimental 110 cycles (TC+DSC). The material can be thus considered to have relatively less stable activation temperature range in solidification than in melting.

The measured melting and solidification enthalpy of sample CC500 was observed to be quite stable, with most of the changes occurring during the first 10 cycles. The fact that almost no changes in the energy stored/released occurred after simulated thermal cycles (performed in air, in a different furnace) suggest minimal effect of both Sn leakage and, as previously discussed, of SnO formation. The actual value of the above enthalpy is of the order of 9 J/g, while calculations based on the nominal amount of amount of Sn and the enthalpy values of Sn melting enthalpy of 52.7±0.1 J/g (lower than the literature value [27]) suggested a value of 21.1 J/g. Since samples with the same nominal composition and obtained by compacting simple mixed powders leading to coarse Sn particles [13] displayed enthalpy in agreement with the actual amount of Sn in samples, a correlation of enthalpy of these FS-PCM to the size of active phase has to be further investigated.

4.3 Application as PCM: advantages and drawbacks

The characterization tests and analyses of Al-40%m Sn produced by compacting and sintering ball-milled Al and Sn powders proved that this alloy has some interesting features for the application as metallic FS-PCM:

- Absence of leakage in simulated service, which is a fundamental point for FS-PCM.
- A narrow activation temperature range in melting, with onset slightly lower than that of pure Sn. The solidification occurs in a broader range at lower temperature. The material has thus the potential for fast energy storage in heating and slow energy release in cooling.
- Relatively good and stable mechanical properties, improved with respect to other manufacturing routes for the same alloy, are beneficial for its use as FS-PCM.
- The thermal response is quite stable after a few initial cycles: microstructural changes occurring during repeated cycles do not alter temperature ranges of the phase transitions and their enthalpy.

Despite of these satisfactory results, the stored/released energy of the material (~ 9 J/g) is lower than expected and further investigations are needed to understand and cope to this feature, critical for its use as Phase Change Material.

5. Summary/Conclusions

1. Al-40%mass Sn alloy was produced by cold compression and sintering of ball milled Al and Sn powders and the properties of interest to its application as metallic form-stable Phase Change Material (PCM) based on Miscibility Gap Alloy (MGA) have been investigated.
2. The Al-Sn alloy obtained had slightly less Sn than nominal composition and, further, it contains some oxygen deriving from ball-milling powders, which forms SnO in the following thermal cycling steps. The microstructure is characterized by the presence of both coarse and fine Sn particles as well as Al grains. High-temperature sintering and thermal cycles induced the formation of a third microstructure, consisting of a fine distribution of sub-micrometric Al and Sn particles, due to Al diffusion in molten Sn. This microstructure increases hardness (~44 HV on average) and helps to prevent leakage of molten Sn during simulated service.
3. Most of the thermal analyses were focused on sample sintered at 500°C for 1 hour, since its microstructural investigation hardness tests revealed as the most promising condition. The analyses were repeated on sample after 100 thermal cycles (175÷285°C), during which only a few Sn droplet formed on the sample surface.

4. According to DSC tests, the studied material can store about 9 J/g at 228°C, keeping a good thermal and mechanical stability during thermal cycles, even if the energy value is lower than expected. Heat storage is relatively fast and repeatable in a temperature range of 10÷20°C; on the other hand, heat release is highly dependent on size distribution of Sn particles, resulting in undercooling and to a more gradual heat release.

Conflict of Interest: The authors declare that they have no conflict of interest.

References

[1] K. Pielichowska, K. Pielichowski, Phase change materials for thermal energy storage, Prog. Mater. Sci. 65 (2014) 67–123. doi:10.1016/J.PMATSCI.2014.03.005.

[2] M.M. Kenisarin, High-temperature phase change materials for thermal energy storage, Renew. Sustain. Energy Rev. 14 (2010) 955–970. doi:10.1016/J.RSER.2009.11.011.

[3] M. Kuta, D. Matuszewska, T.M. Wójcik, The role of phase change materials for the sustainable energy, E3S Web Conf. 10 (2016) 68. doi:10.1051/e3sconf/20161000068.

[4] M. Kuta, T.M. Wójcik, Phase change materials in energy sector - applications and material requirements, EPJ Web Conf. 92 (2015) 2043. doi:10.1051/epjconf/20159202043.

[5] H. Sugo, E. Kisi, D. Cuskelly, Miscibility gap alloys with inverse microstructures and high thermal conductivity for high energy density thermal storage applications, Appl. Therm. Eng. 51 (2013) 1345–1350. doi:10.1016/J.APPLTHERMALENG.2012.11.029.

[6] C. Zhou, S. Wu, Medium- and high-temperature latent heat thermal energy storage: Material database, system review, and corrosivity assessment, Int. J. Energy Res. 43 (2019) 621–661. doi:10.1002/er.4216.

[7] G. Wei, G. Wang, C. Xu, X. Ju, L. Xing, X. Du, Y. Yang, Selection principles and thermophysical properties of high temperature phase change materials for thermal energy storage: A review, Renew. Sustain. Energy Rev. 81 (2018) 1771–1786. doi:10.1016/J.RSER.2017.05.271.

[8] S.A. Mohamed, F.A. Al-Sulaiman, N.I. Ibrahim, M.H. Zahir, A. Al-Ahmed, R. Saidur, B.S. Yılbaş, A.Z. Sahin, A review on current status and challenges of inorganic phase change materials for thermal energy storage systems, Renew. Sustain. Energy Rev. 70 (2017) 1072–1089. doi:10.1016/J.RSER.2016.12.012.

[9] S.P. Singh, B.K. Deb Barman, P. Kumar, Cu-Bi alloys with high volume fraction of Bi: A material potentially suitable for thermal surge protection and energy storage, Mater. Sci. Eng. A. 677 (2016) 140–152. doi:10.1016/J.MSEA.2016.09.041.

[10] S. Reed, H. Sugo, E. Kisi, High temperature thermal storage materials with high energy density and conductivity, Sol. Energy. 163 (2018) 307–314. doi:10.1016/J.SOLENER.2018.02.005.

[11] T. Fiedler, A.J. Rawson, H. Sugo, E. Kisi, Thermal capacitors made from Miscibility Gap Alloys (MGAs), in: WIT Trans. Ecol. Environ., WIT Press, 2014: pp. 479–486. doi:10.2495/ESUS140411.

[12] X. Liu, M.Q. Zeng, Y. Ma, M. Zhu, Promoting the high load-carrying capability of Al–20wt%Sn bearing alloys through creating nanocomposite structure by mechanical alloying, Wear. 294–295 (2012) 387–394. doi:10.1016/j.wear.2012.07.021.

[13] E. Gariboldi, M. Perrin, Metallic Composites as Form-Stable Phase Change Alloys, in: THERMEC 2018, Trans Tech Publications, 2019: pp. 1966–1971. doi:10.4028/www.scientific.net/MSF.941.1966.

[14] C. Suryanarayana, Mechanical alloying and milling, Prog. Mater. Sci. 46 (2001) 1–184. doi:https://doi.org/10.1016/S0079-6425(99)00010-9.

[15] C. Confalonieri, Z. Li, E. Gariboldi, Metallic Form-Stable Phase Change Materials for Thermal Energy Storage and Management: general features and effect of manufacturing process on thermal response and stability, La Metall. Ital. - Int. J. Ital. Assoc. Metall. 7/8 (2019) 12–20.

[16] A. Toda, Heating rate dependence of melting peak temperature examined by DSC of heat flux type, J. Therm. Anal. Calorim. 123 (2016) 1795–1808. doi:10.1007/s10973-015-4603-3.

[17] X. Liu, M.Q. Zeng, Y. Ma, M. Zhu, Melting behavior and the correlation of Sn distribution on hardness in a nanostructured Al–Sn alloy, Mater. Sci. Eng. A. 506 (2009) 1–7. doi:10.1016/J.MSEA.2008.12.054.

[18] H.E. Exner, E. Arzt, Sintering Processes, in: R.W. Cahn, P. Haasen (Eds.), Phys. Metall. (Fourth Ed., Fourth Ed., North-Holland, Oxford, 1996: pp. 2627–2662. doi:https://doi.org/10.1016/B978-044489875-3/50036-3.

[19] S. Gražulis, A. Daškevič, A. Merkys, D. Chateigner, L. Lutterotti, M. Quirós, N.R. Serebryanaya, P. Moeck, R.T. Downs, A. Le Bail, Crystallography Open Database (COD): an open-access collection of crystal structures and platform for world-wide collaboration, Nucleic Acids Res. 40 (2012) D420–D427. doi:10.1093/nar/gkr900.

[20] R.W.G. Wyckoff, Second edition. Interscience Publishers, New York, Cryst. Struct. 1 (1963) 7–237.

[21] L. Lutterotti, Maud, (n.d.). http://maud.radiographema.eu.

[22] W.F. Hemminger, S.M. Sarge, The baseline construction and its influence on the measurement of heat with differential scanning calorimeters, J. Therm. Anal. 37 (1991) 1455–1477. doi:10.1007/BF01913481.

[23] W. Steurer, Crystal Structures of the Elements, Encycl. Mater. Sci. Technol. (2001) 1880–1897. doi:10.1016/B0-08-043152-6/00344-2.

[24] C. Yu, J. Liu, H. Lu, J. Chen, Ab initio calculation of the properties and pressure induced transition of Sn, Solid State Commun. 140 (2006) 538–543. doi:https://doi.org/10.1016/j.ssc.2006.09.026.

[25] A. V Gorokh, I.A. Danilenko, V.B. Primisler, Suppression of Anomalous Allotropic Transformations at High Pressures, Inorg. Mater. 39 (2003) 183–185. doi:10.1023/A:1022154931469.

[26] N. Navarrete, A. Gimeno-Furio, R. Mondragon, L. Hernandez, L. Cabedo, E. Cordoncillo, J.E. Julia, Nanofluid based on self-nanoencapsulated metal/metal alloys phase change materials with tuneable crystallisation temperature, Sci. Rep. 7 (2017) 17580. doi:10.1038/s41598-017-17841-w.

[27] W. Shackelford, James F., Alexander, ed., CRC Materials Science and Engineering Handbook, 3rd ed., CRC Press, Boca Raton, 2001. doi:https://doi.org/10.1201/9781420038408.

[28] W.T. Kim, B. Cantor, Solidification of tin droplets embedded in an aluminium matrix, J. Mater. Sci. 26 (1991) 2868–2878. doi:10.1007/BF01124815.